Journal of Solid State Chemistry **143,** 230–238 (1999)
Article ID jssc.1998.8098, available online at http://www.idealibrary.com on IDEAL®

A New Nasicon-Type Phosphate: $Co_{0.5}Ti_2(PO_4)_3$ II. Simulation of Optical and Magnetic Properties

J. Derouet,[1] L. Beaury, and P. Porcher

Laboratoire de Chimie Appliquée de l'Etat Solide, ENSCP, 11 rue Pierre et Marie Curie, F-75231 Paris Cedex 05, France

R. Olazcuaga, J. M. Dance, and G. Le Flem

Institut de Chimie de la Matière Condensée, CNRS-UPR9048, Av. Dr Schweitzer, F-33608 Pessac, France

and

A. El Bouari and A. El Jazouli

Département de Chimie, Faculté des Sciences M'Sik Sidi Othmane, BP 6621 Casablanca, Morocco

Received February 28, 1997, in revised form November 4, 1998, accepted December 7, 1998

The optical (energy level scheme) and magnetic properties (paramagnetic susceptibility as a function of the temperature and *g* values) of the polycrystalline $Co_{0.5}Ti_2(PO_4)_3$ were simultaneously reproduced by use of a crystal field theory involving a set of F^k,ζ, free ion, and B_q^k crystal field parameters. The crystal field parameters calculated from the structure are in fair agreement with the experimental ones and permit us to assign *R*32 as the space group of the crystal structure. © 1999 Academic Press

INTRODUCTION

The simulation of the electron configurations of the rare earths has received considerable attention for 30 years. A great number of transitions are usually recorded by both absorption and emission techniques. The transitions are narrow and well defined, permitting the construction of an energy level scheme of more than 100 crystal field levels. The spectrum provides an experimental basis for an accurate simulation of the electron configurations, in which various interactions are recognized and parameterized. In addition to the classical electrostatic repulsion, spin–orbit coupling, and crystal field interaction, others of smaller impact, like two- and three-body interactions, together with magnetic ones, can be introduced. It is general practice to conduct the simulation of the $4f^N$ configurations with about 20 phenomenological parameters (1). Nevertheless, attention was initially focused on the $3d^N$ electron configurations, since most of the theories were based on the optical results of these configurations. The low number of observed energy levels, as well as the strong electron-phonon coupling, together with the lack of powerful computers forced the scientists of that time to simplify the theory and to apply the perturbation theory. The $|SM_SLM_L\rangle$ basis was used instead of the $|SLJM\rangle$ one for the rare earths; i.e., the spin-orbit interaction was neglected even though the spin-orbit coupling constant could be estimated later. The D_q cubic crystal field parameter was also introduced instead of the individual B_q^k's. As time progressed practical approaches to the treatment of the $3d^N$ and $4f^N$ configurations evolved. The aim of the work is to apply the simulation process for the $4f^N$ configuration to the $3d^7$ configuration of the divalent cobalt in $Co_{0.5}Ti_2(PO_4)_3$, for which the optical as well as some of the magnetic properties were reported in Part 1 (2). The calculation of B_q^k will be discussed with respect to the oxygen environment of the cobalt (SOM model). The diversity of the experimental data for this compound, in which the cobalt occupies a pseudo-octahedral site, permits testing the reliability of the theories which are employed and establishing a correlation between crystallography and crystal field. The process of simulation differs from the rare earth case, because the optical data cannot be considered by themselves but the EPR data and paramagnetic susceptibility as a function of temperature must be included as well. In the case of EPR, and for a best determination of the crystal field parameters, a knowledge of the *g* factors' anisotropy is necessary. It is determined by a study of $Mg_{0.49}Co_{0.01}Ti_2(PO_4)_3$ since the undoped compound yields only the *g* average value. If

[1]To whom correspondence should be addressed: Chimie Appliquée de l'Etat Solide-ENSCP, 11 rue Pierre et Marie Curie, F-75231 Paris Cedex 05, France. Fax: 33 (0) 1 46 34 74 89. E-mail: beaury@ext.jussieu.fr.

0022-4596/99 $30.00
Copyright © 1999 by Academic Press
All rights of reproduction in any form reserved.

these conditions are met, an accurate simulation can be carried out.

THEORETICAL BACKGROUND

1. $3d^N$ Electron Configurations

The description of an electron configuration is based on the one center model. The electrons are supposed to move independently from each other and are subject to various independent interactions. Their effects are represented by nonzero matrix elements between the $|SLJM\rangle$ states of the configuration. The quantitative effect of the interaction is usually described according to Racah algebra techniques. This method, comprehensively described in (3), has been extensively used for the simulation of the nf^N configurations of the rare earth and of the actinide ions (4). The hamiltonian including the different interactions may be written as:

$$H_{TOT} = H_0 + H_{CR} + H_{SO} + H_{CF},$$

where

— H_0 is the spherically symmetric one-electron part of the free-ion hamiltonian which separates the ground configuration from the excited ones.

— $H_{CR} = \sum_{k=0,2,4} F^k(nd, nd) f_k$ represents the coulombic repulsion, in which F^k are the Slater integrals, considered as phenomenological parameters, and f_k denotes the angular parts of the electrostatic repulsion. As an alternative expression of this interaction one may introduce the Racah parameters B and C, a linear combination of the Slater integrals.

— $H_{SO} = \zeta\ A_{SO}$ is the spin–orbit interaction, where ζ is the spin–orbit coupling constant and A_{SO} its angular part.

— H_{CF}, the one-electron crystal-field hamiltonian, consists of a sum of products between the crystal-field parameters (cfps) and the spherical harmonics C_q^k:

$$H_{CF} = \sum_{k=0}^{4} \sum_{q=0}^{k} B_q^k [C_q^k + (-1)^q C_{-q}^k] + iS_q^k [C_q^k - (-1)^q C_{-q}^k]$$

In that expression B_q^k and S_q^k represent the real and imaginary part of the cfps. The number of the nonzero parameters depends on the crystallographic point site symmetry. For the C_{3v} or S_6 point symmetries considered in Part I (2), the even terms of the crystal field hamiltonian are the same

$$H_{C_{3v}} = B_0^2 C_0^2 + B_0^4 C_0^4 + B_3^4 (C_3^4 - C_{-3}^4),$$

whereas the imaginary parameters are present in the C_3 symmetry:

$$H_{C_3} = H_{C_{3v}} + iS_3^4 (C_3^4 + C_{-3}^4).$$

The latter expression will not be used because an appropriate rotation of the reference axis system around z causes the imaginary parameter to vanish. The difference between $H_{C_{3v}}$ and H_{S_6} lies in the odd terms of the crystal field. For S_6, the odd terms vanish and all electric dipole transitions are forbidden. Only the magnetic dipole and phonon assisted transitions remain. Moreover, the simulation of the $3d^N$ configurations frequently requires use of the descending symmetry procedure, starting from the cubic symmetry, which involves only the crystal field parameter D_q, directly related to B_0^4 by $B_0^4 = -14\,D_q$ for ternary symmetry ($B_0^4 = 21\,D_q$ for quaternary symmetry). The B_0^2 value and the deviation of the B_3^4/B_0^4 ratio from the cubic symmetry ($B_3^4/B_0^4 = -1.195$) characterize the axial distorsion.

The main differences between $3d^N$ and $4f^N$ (or $5f^N$) configurations lie in: (i) the number of parameters introduced by H_{CR} and H_{CF} interactions and (ii) the order or magnitude of these interactions. For the $3d$ elements the crystal field strength can be tens of times greater than for the $4f$ elements, whereas H_{CR} is of the same order of magnitude, and H_{SO} smaller, which explains why the $|SM_SLM_L\rangle$basis can often replace the $|SLJM\rangle$one to facilitate the calculations.

2. Paramagnetic Susceptibility and Effective Magnetic Moment

According to the work of van Vleck (5), the paramagnetic susceptibility χ as a function of temperature is written as

$$\chi = \frac{N\beta^2}{\sum_i \exp -\left(\frac{E_i^{(0)}}{kT}\right)} \sum_i \left[\frac{(\varepsilon_i^{(1)})^2}{kT} - 2\varepsilon_i^{(2)}\right] \exp -\left(\frac{E_i^{(0)}}{kT}\right)$$

with

$$\varepsilon_i^{(1)} = \langle \Psi_i | (\mathbf{L} + g_e \mathbf{S}).\mathbf{u} | \Psi_i \rangle$$

and

$$\varepsilon_i^{(2)} = \sum_{\substack{j \\ E_i^{(0)} \neq E_j^{(0)}}} \frac{[\langle \Psi_i | (\mathbf{L} + g_e \mathbf{S}).\mathbf{u} | \Psi_j \rangle]^2}{E_i^{(0)} - E_j^{(0)}}$$

In these expressions, N is Avogadro's number, k the Boltzmann constant, μ_B the Bohr magneton and $g_e = 2.0023$. The wavefunctions ψ_i and ψ_i are the eigenfunctions, unperturbed by the magnetic field, corresponding to the eigenvalues $E_i^{(0)}, E_j^{(0)}$. $\mathbf{u}$ is a unit vector describing the three components of the magnetic dipole tensor, related to the susceptibilities χ_x, χ_y, and χ_z (or $\chi_{//}$ and $\chi_\perp$ for axial symmetry).

For $3d^N$ elements, the effective magnetic moment μ_{eff} and its evolution *vs* temperature is traditionally preferred

instead of χ. The relationship to χ is

$$\mu_{\text{eff}} = 2.828\sqrt{\chi_{\text{av}}T} \text{ Bohr magnetons.}$$

3. Magnetic Splitting Factors g

The principle for calculation the g value is quite similar to that of the paramagnetic susceptibility. The same $(\mathbf{L} + g_e\mathbf{S})$ tensorial operator is applied to the unperturbed wavefunction. The g values are nonzero only for Kramers doublets. For axial symmetry, only $g_{//}$ (parallel to the symmetry axis) and $g_\perp$ are used:

$$g_{//} = g_z = 2[\langle\psi_+|L_z + g_eS_z|\psi_+\rangle^2 + \langle\psi_+|L_z + g_eS_z|\psi_-\rangle^2]^{1/2}$$

$$g_\perp = g_x = 2[\langle\psi_+|L_x + S_x|\psi_-\rangle] = g_y.$$

In these expressions, ψ_+ is an eigenvector of the form

$$\psi_+ = a|J, M\rangle + b|J, M'\rangle + , \ldots ,$$

whereas ψ_- is its Kramers conjugate

$$\psi_- = (-1)^{J+M}a^*|J, -M\rangle + (-1)^{J+M'}b^*|J, -M'\rangle + \ \ldots$$

Such expressions could be replaced by direct calculation if the magnetic interaction is introduced in the secular determinant before diagonalization (6).

PHENOMENOLOGICAL SIMULATION

The aim of the present simulation is to consider simultaneously the optical and magnetic data and to reproduce these data by using a reduced number of phenomenological parameters. The $3d^7$ configuration of Co^{2+} involves 120 $|\text{SLJM}>$ kets. Due to the odd number of electrons the number of levels is reduced to 60 Kramers doublets in the absence of a magnetic field. The number of involved parameters consists of three free ion (F^2, F^4, and ζ) and three crystal field parameters (B_0^2, B_0^4, and B_3^4). Contrary to the rare earth electron configurations, for which the number of experimental levels largely exceeds the number of parameters, the number of levels observed here is relatively low and frequently the positions are not accurate, due to the electron–phonon coupling and to the relatively small spin–orbit coupling. Consquently, the energy level sequence is used as a guiding principle for the simulation, whereas the most important data come from the paramagnetic susceptibility and its behavior as a function of temperature, as well as from the magnetic splitting g factors. A knowledge of the anisotropy of g values is essential. For a polycrystalline compound, only the EPR measurements yield this type of information.

The simulation proceeds as follows:

— in the first step, only one free ion parameter (B) and one crystal field parameter (B_0^4 or D_q) are considered. An approximate value is directly determined from the selected spin allowed transitions (7): $^4T_{1g}(^4F) \rightarrow {}^4T_{2g}(^4F)$, $^4A_{2g}(^4F)$, $^4T_{1g}(^4P)$. The spin–orbit coupling constant is fixed at 450 cm^{-1}, corresponding to the reduced value of that of the free ion. The other free ion parameter C is related to B by the hydrogenic ratio $C \cong 4B$ (8, 9).

— in the second step of the simulation one assumes that B_3^4 varies independent of B_0^4 but is close to the cubic ratio, as indicated by semi-empirical calculations ($B_3^4/B_0^4 \cong -1$); also B and C vary around their hydrogenic ratio, although the C value can be determined from the spin forbidden transitions.

— in the last step all parameters vary freely.

In such simulation we move in a six-dimensional space where each set of parameters determines the eigenvalues and eigenvectors which diagonalize the total hamiltonian without magnetic field (10–12). Because the free ion and the crystal field interactions have the same order of magnitude, the procedure is more complicated than for the rare earth ions. The simulation also has to agree with the external conditions (here semi-empirical calculations) in order to maximize our confidence in it. Within this frame work and by using the process indicated above, a set of parameters was found which reproduce all the data reasonably well (Table 1).

SEMIEMPIRICAL CALCULATIONS

1. The Simple Overlap Model

The crystal field parameters can be theoretically calculated from the atomic positions in the structure. If the simple point charge electrostatic model (PCEM) (13) is unable to represent reasonably the experimental values, some more sophisticated models can be used, such as the angular overlap model AOM (14) and the effective charge model ECM (15). The former only considers the first coordination sphere and some intrinsic parameters related to the nature of the ligand. The latter model sums the contributions of all atoms in the crystallographic network. The number of atoms to be taken into account depends on the rank of the parameter to be calculated. For the B_q^4 parameters the radius of the sphere is *circa* 30 Å, whereas a radius of *ca* 100 Å is required for the B_q^2 before converging values could be obtained. The more recent simple overlap model (SOM) developed by Malta (16, 17) has been successfully applied to reproduce the phenomenological cfps for a great number of lanthanides, as well as for some $3d$ element compounds (18–20).

In the SOM model one supposes that the crystal field effect can be calculated by assuming a potential produced by an effective charge distribution over a small region,

TABLE 1
$Co_{1/2}Ti_2(PO_4)_3$-Parameters (cm^{-1}), μ_{eff} (BM), g Values

			Semi-empirical calculation							
	Exp.	Opt. fit C_{3v}	$R32$				$R\bar{3}$			
ρ	—	—	0.14		0.16		0.14		0.16	
g_0[a]	—	—	− 1.2	− 1.1	− 0.9	− 0.8	− 1.1	− 1.0	− 0.9	− 0.8
F^2		69186	68866	68692	68872	68925	69437	68376	68189	68503
F^4		46307	48436	47550	48449	47117	47907	48088	49193	47653
ζ		[450]	[450]	[450]	[450]	[450]	[450]	[450]	[450]	[450]
B_0^2		− 8877	11228	10558	11195	10373	14013	12739	14061	12499
B_0^4	− 11410	− 11671	− 11850	− 11002	− 11862	− 10772	− 12144	− 11022	− 12752	− 11336
B_3^4	13638	12676	10657	9894	10662	9606	11166	10134	11719	10422
B_3^4/B_0^4	Cub.	− 1.09	− 0.90	− 0.90	− 0.90	− 0.90	− 0.92	− 0.92	− 0.92	− 0.92
rms dev.		115	128	172	127	235	114	250	270	230
B	833	872	856	863	856	872	874	850	834	858
C		3780	3844	3774	3845	3739	3802	3817	3904	3782
C/B		4.33	4.49	4.37	4.49	4.29	4.35	4.49	4.68	4.41
D_q	815	834	846	786	847	769	867	787	911	810
μ_{eff} (5 K)	3.95	4.07	3.77	3.79	3.77	3.81	4.07	3.89	4.12	3.83
μ_{eff} (100 K)	4.75	4.70	4.64	4.71	4.64	4.75	4.40	4.48	4.36	4.49
μ_{eff} (300 K)	4.97	4.91	4.80	4.90	4.81	4.97	4.48	4.58	4.44	4.60
$\lvert g_{//}\rvert$	7.34	7.44	2.44	2.58	2.45	2.71	2.27	2.27	2.19	2.28
$\lvert g_{\perp}\rvert$	2.11	2.11	4.80	4.85	4.81	4.87	4.54	4.63	4.51	4.66
g_{av}[b]	4.57	4.63	4.16	4.23	4.17	4.27	3.93	4.00	3.89	4.03

[a] g, effective charge of oxygen.
[b] g_{av}, $\frac{1}{3}(g_{//}^2 + 2g_{\perp}^2)$.

proportional to overlap integrals and situated at the mid-point of the metal–ligand distance. One calculates the B_q^k parameters using the relation

$$B_q^k = \rho\left(\frac{2}{1 \pm \rho}\right)^{k+1} A_q^k \langle r^k \rangle,$$

where A_q^k is the lattice sum of neighbors belonging to the first coordination sphere associated with an effective charge, $\langle r^k \rangle$ are the radial integrals (for the cobalt, $\langle r^2 \rangle$ and $\langle r^4 \rangle$ are equal to 1.2587 (a.u.)^2 and 3.706 (a.u.)^4, respectively (21)), ρ is the overlap between the $3d$ orbitals of the central ion, and the s and p orbitals of the ligand, the value of which varies as a function of the metal–ligand distance R, according to an exponential law $\rho = \rho_0(R_0/R)^n$, R_0 being the shortest metal–ligand distance and $2.5 \leq n \leq 5$.

The $\pm$ sign indicates the relative covalency when different ligands exist and characterizes the displacement of the charge barycenter from the metal–ligand mid-distance (22). If we consider that the $3d$ orbitals are expanded due to penetrating ligand orbitals and that the $3d$–$4s$ mixing may be very important, it is not unrealistic to consider ρ values between 0.10 and 0.30. The overlap integrals are larger for the $3d^N$ elements than for the lanthanide compounds, for which ρ is in the range 0.05 to 0.08 (19, 23). The simple overlap model may be regarded as a starting point to carry out practical crystal field calculations.

2. *Application to $Co_{0.5}Ti_2(PO_4)_3$*

In order to calculate the cfps in the trigonal symmetry of cobalt in $Co_{0.5}Ti_2(PO_4)_3$, a systematic assessment of the three-dimensional space involving the B_q^k, the oxygen effective charge g_0, and the overlap was done for the two possible crystallographic groups $R\bar{3}$ and $R32$ (Part I) (2). In the beginning, the calculation was performed in the large overlap ($0.10 < \rho < 0.20$) and effective charge ($-2 < g_0 < -0.6$) domain, which are the ranges in which the best agreement with the phenomenological value is expected. From a chemical point of view, the cobalt–oxygen bonding is supposed to be relatively ionic, because the $[Ti_2(PO_4)_3]$ skeleton is covalent. This is the reason why the oxygen effective charge range can be restricted to $-1.2 < g_0 < -0.8$. These values are very close to the effective charges found for oxygen ligands of lanthanide compounds (15). Figure 1 presents the results of calculations concerning the main parameter B_0^4 for both possible space groups $R\bar{3}$ and

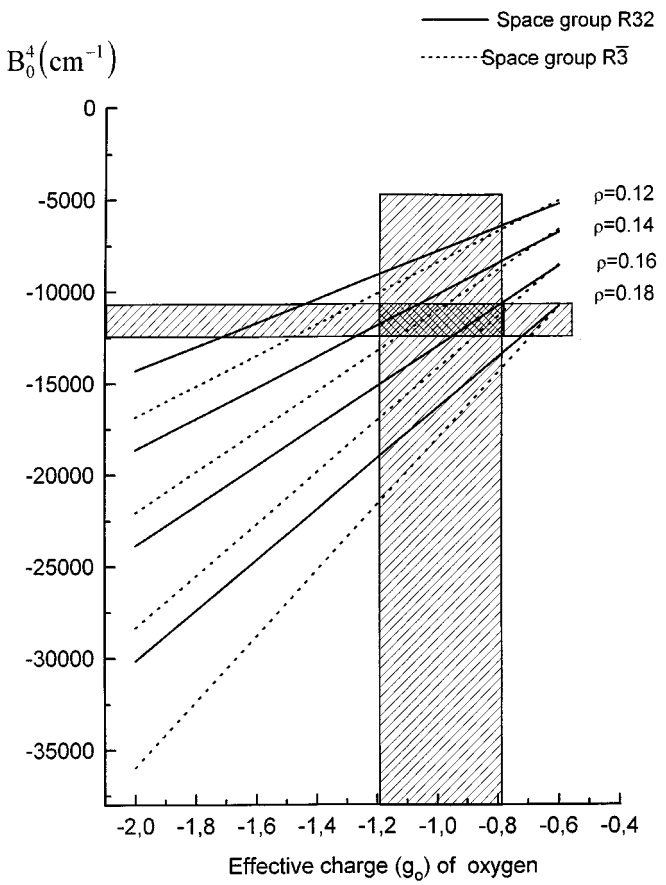

FIG. 1. Variation of B_0^4 versus the oxygen effective charge for the two space groups $R32$ and $R\bar{3}$ and for different overlaps $0.12 \leq \rho \leq 0.18$. The double hatched part indicates the area of possible values for B_0^4 and ρ.

$R32$. To keep B_0^4 within the experimental value range, ρ must be close to 0.15 ($\rho = 0.14$ and $\rho = 0.16$ in Table 1), which also reproduces well the relative ionicity of the bonding.

The energy level scheme of Co^{2+} was derived from the diagonalization after introducing the calculated B_q^k's, together with standard values for the free ion parameters (9) in the secular determinant. The curves in Fig. 2 reproduce the variation of the energy levels' positions as a function of effective charge of the oxygen, through the B_q^k's values. A high mixing between the nominal states is obtained, and it is practically impossible to characterize an energy level only with a single $|SLJM\rangle$ set. The wavefunctions associated with each energy level are in fact linear combinations of all the states in the configuration basis, the only selections conforming to the group theory rules. This divides the secular determinant into smaller ones according to the crystal quantum number (24), also separating the point group irreducible representations. For example, the main contributions in the $|\text{“}^4P\text{”}\rangle$ level wavefunction ($\sim 20000\ cm^{-1}$) are

$$39.82\%|^4P3/2, 1/2\rangle + 12.11\%|^2P3/2, 1/2\rangle + 9.99\%|^2P1/2, 1/2\rangle + \ldots$$

$$\text{that is } 51.22\%|^4P, {}^4F\rangle + 48.78\%|^2P, {}^2G, {}^2H, {}^2D\rangle$$

Each curve in Fig. 2 also reproduces the approximate experimental spectrum, which permits us to select a relatively well-defined effective charge, even if the phonon coupling does not permit us to determine unambiguously the position of the zero-phonon line. Finally, this calculation alone does not lead to an unambigous decision between the two point groups.

When the magnetic properties are considered, the variation of the effective moment μ_{eff} as a function of temperature is different for the two point groups. The best agreement between the calculated and experimental curves is obtained for $\rho = 0.16$ and $g_0 = -0.8$, as well as for $\rho = 0.14$ and $g_0 = -1.1$ for the $R32$ space group (Fig. 3). At this point, it should be assumed that the ambiguity concerning the space group is lifted. However, the calculated $g_{//}$ and $g_\perp$ values are in disagreement with the experiment; hence, a systematic analysis of the g values as a function of the wavefunction composition has been performed.

THE g VALUES AND THE WAVEFUNCTION COMPOSITION

It has been shown elsewhere that $g_{//}$ and $g_\perp$ values of the ground state are very sensitive to the wavefunction composition, i.e., to the values of the crystal field parameters (25, 26). Therefore, a systematic analysis of the variation of the g values was carried out. Figure 4a presents the variation of the g values when the B_3^4/B_0^4 ratio is distorted from the cubic value. In that case, it is assumed that the value of B_0^4 is close to the "experimental" one and also corresponds to the one calculated by SOM with an overlap of 0.14 (Table 1). At that point, B_0^2 is fixed to zero. The intersection of the two curves is obtained when the B_3^4/B_0^4 ratio assumes the cubic value (-1.195). The best region of agreement is found for $B_3^4/B_0^4 \sim -1.0$, which is also close to the ratio calculated by SOM (-0.90) for the $R32$ point group. The second step (Fig. 4b) studies the effect of B_0^2 when the ratio B_3^4/B_0^4 is fixed to -0.90. Position 1 corresponds to the SOM calculated B_0^2. For this set of calculated parameters, the energy level scheme and the magnetic effective moment μ_{eff} as a function of temperature (Fig. 3, curve $R32$), as well as the average g value (measured on the "pure" Co compound) were well reproduced. The only mismatch concerns the g anisotropy for the doped Co compound. To reproduce the anisotropy requires a negative value for B_0^2, far from the one calculated by SOM (position 2 in Fig. 4b). An intermediate position with $B_0^2 \sim 5000\ cm^{-1}$ should reproduce well the anisotropy,

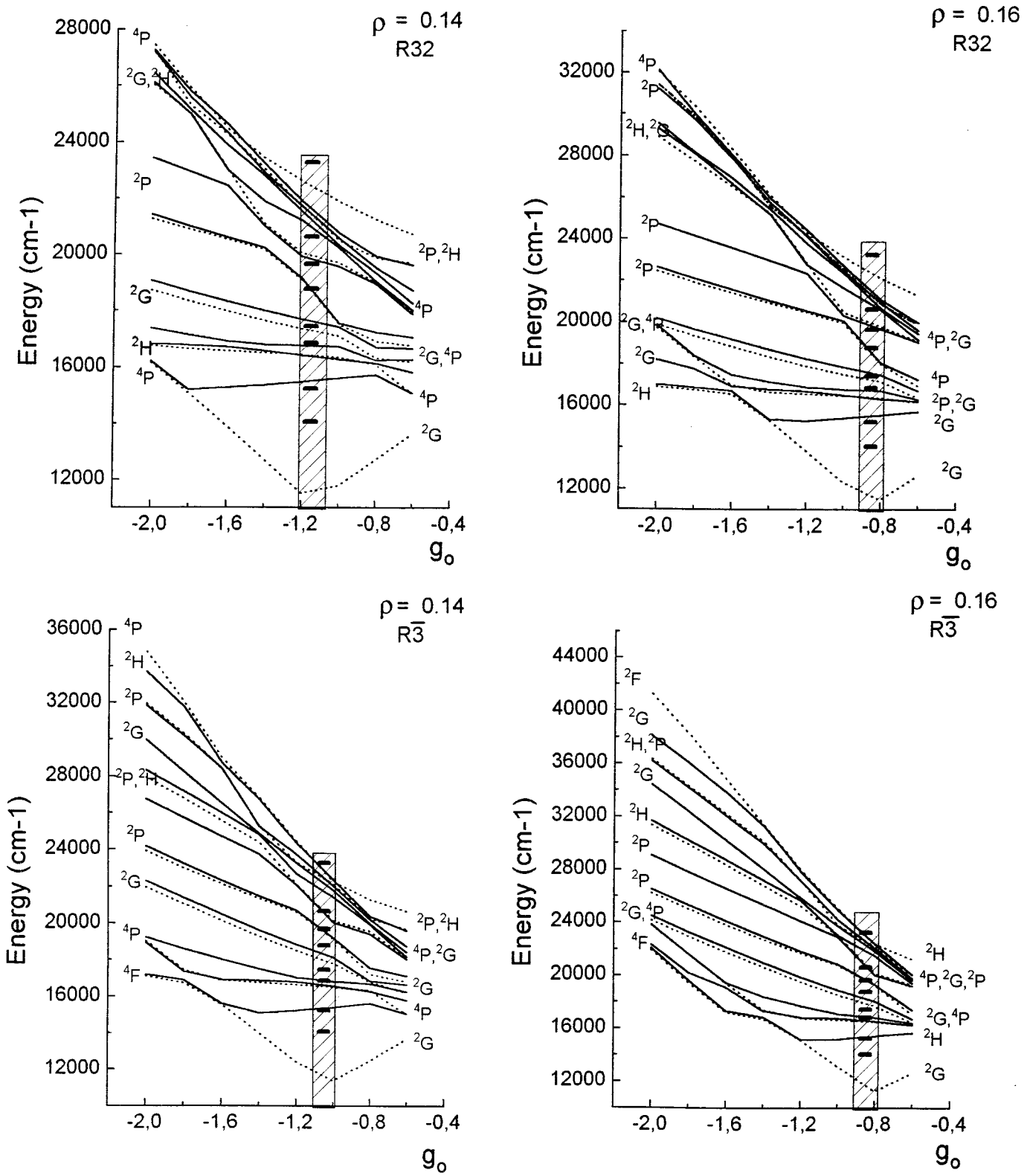

FIG. 2. Calculated energy level schemes vs the oxygen effective charge g_0, in the case of $R32$ and $R\bar{3}$ for two overlaps ($\rho = 0.14$ and $\rho = 0.16$). The solid lines (resp., dotted line) correspond to the $D_{1/2}$ (resp., $S_1 + S_3$) irreducible representations. The hatched regions delimit the most probable g_0 value and contains the experimentally observed absorption energy levels.

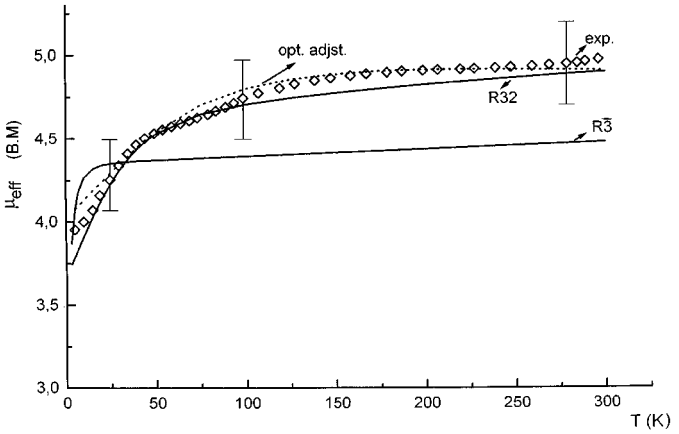

FIG. 3. Experimental (diamonds, error bars $\pm 5\%$) and calculated paramagnetic susceptibility curves versus temperature. (—). From semi-empirical B_q^k parameters for the $R32$ ($\rho = 0.14$, $g_0 = -1.1$) and $R\bar{3}$ ($\rho = 0.14, g_0 = -1$) space groups. ($\cdots$). From phenomenological B_q^k parameters.

but results in a μ_{eff} far from the experiment. After varying the B_3^4/B_0^4 ratio around the value calculated by SOM, a satisfactory solution has been found with $B_3^4/B_0^4 \sim -1.1$ (Fig. 4c). When B_0^2 is added to the calculation, the best solution reproducing simultaneously the energy level scheme, μ_{eff}, g_{av} and the g anisotropy is found for $B_0^2 \approx -9000\,\text{cm}^{-1}$. This is close to the value when the crystal field parameters vary freely in the phenomenological simulation of the energy level scheme (Tables 1 and 2).

CONCLUSION

For $Co_{0.5}Ti_2(PO_4)_3$ the B_0^2, B_0^4, B_3^4 crystal field parameters were calculated approximately from the optical absorption (phenomenological simulation) and from the SOM model (semi-empirical calculation). The latter model gives the starting values for a new refining procedure. However, the crystallographic model permits us to choose between the two possible space groups of the structure. In both cases the calculation takes into account all the states of the $3d^7$ configuration and the agreement with experimental energy level scheme, as well as the paramagnetic susceptibility, can be regarded as satisfactory. On the other hand, the g values are calculated only from the composition of the ground state wavefunction which results (in the high spin situation) principally through the mixing of the lowest level (^4F) with the upper (^4P) term of the same symmetry. The degree of mixing is very sensitive to the influence of the crystal field. This could be one explanation as to why, for the anisotropy of the g values, the sign of B_0^2 remains ambiguous.

In the SOM model the effective charges are proportional to the magnitude of the overlap between the metal $3d$ and ligand orbitals. The contribution from more distant

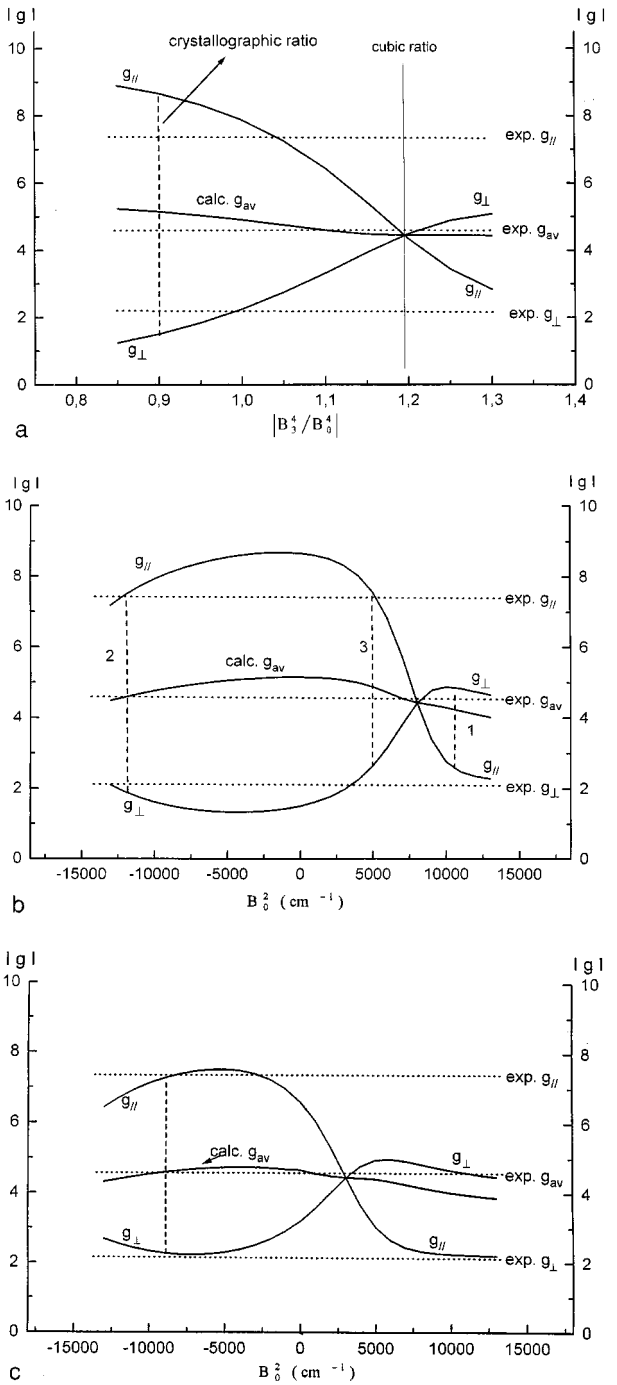

FIG. 4. (a) Calculated $|g|$ factors vs the $|B_3^4/B_0^4|$ ratio ($R32$ space group, $\rho = 0.14$, $B_0^2 = 0$). (b, c) Influence of B_0^2 on the $|g|$ factors for two B_3^4/B_0^4 ratios: (b) $B_3^4/B_0^4 = -0.9$ (calculated ratio), where, The dashed segment 1 corresponds to the calculated B_0^2 ($B_0^2 = 10558\,\text{cm}^{-1}$), the dashed segment 2 gives an acceptable g anisotropy but with $B_0^2 < 0$, and the dashed segment 3 corresponds to an intermediate value of g anisotropy with $B_0^2 = 5000\,\text{cm}^{-1}$. (c) $B_3^4/B_0^4 = -1.1$ (phenomenological ratio). The dashed segment ($B_0^2 = -9000\,\text{cm}^{-1}$) corresponds to the parameters set allowing the simultaneous reproduction of the energy levels scheme, μ_{eff}, g_{av}, and the g anisotropy.

TABLE 2

Evolution of the Calculated μ_{eff} and g Values As a Function of the B_3^4/B_0^4 Ratio and the B_0^2 Value. The Crystallographic Ratio −0.9 is Determined by SOM for the *R*32 Space Group ($\rho = 0.14$, $g_0 = -1.1$)

	Exp.	Opt. fit (C_{3v})	Calc.		
B_3^4/B_0^4	—	− 1.09	− 0.9 (Crystallographic ratio)		− 1.09
B_0^2 (cm^{-1})	—	− 8877	10558	5000	− 8930
μ_{eff} (5 K)	3.95	4.07	3.79	4.27	4.04
μ_{eff} (100 K)	4.75	4.70	4.71	5.06	4.80
μ_{eff} (300 K)	4.97	4.91	4.90	5.41	4.92
$\lvert g_{//}\rvert$	7.34	7.44	2.58	7.55	7.28
$\lvert g_{\perp}\rvert$	2.11	2.11	4.85	2.65	2.26
g_{av}	4.57	4.63	4.23	4.87	4.58

neighbors is important for the low rank ($k = 2$) parameters. In this case the bonding effects are therefore emphasized. For $Co_{0.5}Ti_2(PO_4)_3$ they are characterized by a high absolute value of B_0^2, also obtained from the fitting of optical data. Apparently, the contribution from more distant neighbors cannot explain the sign discrepancy. This problem is too complicated to have a simple solution because the simulation operates in a multidimensional space, corresponding to all interactions to be included in the simulation.

As expected, a precise specification of the interactions is necessary to integrate in the simulation of the $3d^N$ electron configuration, as for the rare earth configurations. The main difference is that the number of experimental energy levels does not greatly exceed the number of parameters, contrary to the case of the $4f^N$ configurations. Consequently, the calculated paramagnetic susceptibility and the g values have to be included in the simulation process by comparing them to the experimental values. A simulation will be satisfactory only when a simultaneous agreement will be found between the different calculations and experiments.

APPENDIX

By analogy with Griffith's diagram (Part I) (2) we have calculated $g_{\perp}$ versus $g_{//}$ for a trigonal symmetry. The g values lie within a fairly narrow region between weak field and strong field limits. The distorsion from trigonal symmetry is characterized by the deviation of the B_3^4/B_0^4 ratio from cubic symmetry ($B_3^4/B_0^4 = -1.195$) and the magnitude of the crystal field parameter B_0^2, about which one has reliable semi-empirical information. In this case we observed a divergence of the calculated curves from the B_3^4/B_0^4 ratio when the parameter B_0^2 is added. The experimental g values for $Co_{0.5}Ti_2(PO_4)_3$ are marked in Fig. 5. If we compare our calculations with these carried out by Griffith or Abragam and Pryce (27,28), the trends are the same but the calculated values are slightly different. The reason is that the calculations proceed from two different approaches.

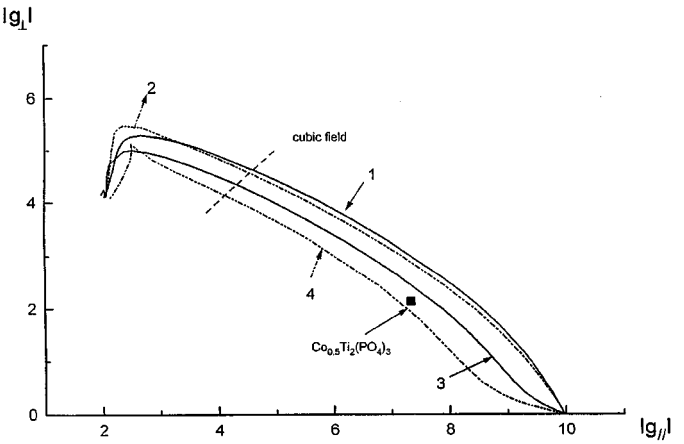

FIG. 5. Variation of $g_{\perp}$ versus $g_{//}$ when the B_3^4/B_0^4 ratio varies: (a) $B_0^2 = 0$ for the two cases: weak field, $B_0^4 = -5000\ cm^{-1}$ (solid line 1) and strong field, $B_0^4 = -19000\ cm^{-1}$ (solid line 3). (b) $B_0^2 < 0$ for the same cases with, respectively, $B_0^2 = -4800\ cm^{-1}$ (dashed line 2) and $B_0^2 = -10558\ cm^{-1}$ (dashed line 4).

REFERENCES

1. L. Beaury, J. Derouet, M. Escorne, and P. Porcher, *J. Phys.: Condens. Matter* **6,** 5169 (1994).
2. J. Derouet, L. Beaury, P. Porcher, R. Olazcuaga, J. M. Dance, G. Le Flem, M. El Bouari, and A. El Jazouli, *J. Solid State Chem.* **143,** 224 (1999).
3. B. G. Wybourne, "Spectroscopic Properties of Rare Earths Ions," Interscience, New York, 1965.
4. W. T. Carnall, G. L. Goodmann, K. Rajnak, and R. S. Rana, "A Systematic Analysis of the Lanthanides Doped into Single Crystal of LaF_3," Argonne National Laboratory Report, 1988.
5. J. H. Van Vleck, *J. Appl. Phys.* **39,** 365 (1968).
6. M. Couto Dos Santos, P. Porcher, *J. Phys.: Condens. Matter* **8,** 4643 (1996).
7. E. König, *Struct. Bond.* (*Berlin*) **9,** 175 (1971).
8. F. E. Mabbs and D. J. Machin, "Magnetism and Transition Metal Complexes," Chapman & Hall, London, 1973.
9. B. N. Figgis, "Introduction to Ligand Fields," Interscience, New York, 1966.
10. P. Caro, J. Derouet and P. Porcher, *C. R. Acad. Sci.* (*Paris*) *Ser. II* **301,** 901 (1985).
11. P. Porcher, *Phase Trans.* **13,** 233 (1988).
12. J. Derouet and P. Caro, *C. R. Acad. Sci.* (*Paris*) *Ser. II* **312,** 605 (1991).
13. H. Bethe, *Ann. Phys.* **3,** 133 (1929).
14. C. E. Schäffer, *Struct. Bond* (*Berlin*) **14,** 69 (1972).
15. C. A. Morrison, R. P. Leavitt, "Handbook of Rare Earths" (K. A. Gschneidner and L. Eyring, Eds.), Vol. 5, p. 461. North Holland, Amsterdam, 1982.
16. O. L. Malta, *Chem. Phys. Lett.* **87,** 27 (1982).
17. O. L. Malta, *Chem. Phys. Lett.* **88,** 353 (1982).
18. O. L. Malta and G. F. De Sa, *Quim. Nova* (*Brazil*) **6,** 123 (1983).
19. O. L. Malta, S. L. J. Ribeiro, M. Faucher, and P. Porcher, *J. Phys. Chem. Solids* **52,** 587 (1991).

20. P. Porcher, M. Couto Dos Santos, and O. Malta, *Phys. Chem. Chem. Phys.* **1** (1999), in press.
21. S. Fraga, J. Karkowski and K. M. S. Saxena, "Handbook of Atomic Data," Elsevier, Amsterdam, 1976.
22. G. P. Barnett, M. C. Pires Costa, and R. Ferreira, *Chem. Phys. Lett*., **25,** 49 (1974).
23. G. Burns, *J. Chem. Phys.* **42,** 377 (1965).
24. K. H. Hellwege, *Ann. Physik*, **4,** 95 (1949).
25. L. Beaury, J. Derouet, P. Porcher, P. Caro, and P. Feldmann, J. Less-Common Met. **126,** 263 (1986).
26. P. Caro, J. Derouet, M. Belkhiria, M. Benamara, M. Dasbabi, J. M. Dance, and G. Le Flem, *J. Chim. Phys.* (*Paris*) **91,** 293 (1991).
27. A. Abragam and M.H.L. Pryce, *Proc. Roy. Soc.* (*London*), *A* **206,** 153 (1951).
28. J. S. Griffith, "The Theory of Transition Metal Ions," Cambridge Univ. Press, Cambridge, UK, 1964.